Author Contributions:
Formal analysis: Xiaofan Li, Zeng-Zhen Hu
Funding acquisition: Xiaofan Li
Methodology: Zeng-Zhen Hu
Supervision: Zeng-Zhen Hu
Writing – original draft: Xiaofan Li
Writing – review & editing: Zeng-Zhen Hu, Yu-heng Tseng, Yunyun Liu, Ping Liang

A Historical Perspective of the La Niña Event in 2020/2021

Xiaofan Li[1,2] ![ORCID], Zeng-Zhen Hu[3] ![ORCID], Yu-heng Tseng[4] ![ORCID], Yunyun Liu[5] ![ORCID], and Ping Liang[6]

[1]Key Laboratory of Geoscience Big Data and Deep Resource of Zhejiang Province, School of Earth Sciences, Zhejiang University, Hangzhou, China, [2]Southern Marine Science and Engineering Guangdong Laboratory, Zhuhai, China, [3]Climate Prediction Center, NCEP/NWS/NOAA, College Park, MD, USA, [4]Institute of Oceanography, National Taiwan University, Taipei, Taiwan, [5]Laboratory of Climate Studies, National Climate Center, China Meteorological Administration, Beijing, China, [6]Key Laboratory of Cities' Mitigation and Adaptation to Climate Change in Shanghai, Shanghai Regional Climate Center, China Meteorological Administration, Shanghai, China

Abstract El Niño–Southern Oscillation is the strongest interannual variability in the tropical oceans and the major source of global climate predictability. In this work, we examine the evolution of oceanic and atmospheric anomalies in the tropical Pacific during 2020/2021 La Niña and compare it with the historical strong La Niña events since 1982, identify the contributions of different time scale components, and assess the predictions and the impact on extra-tropical climate. 2020/2021 La Niña emerged in August 2020 and dissipated in May 2021. 2020/2021 La Niña was uniquely preceded by a borderline El Niño instead of an El Niño and a weak equatorial-heat discharge process. That resulted in the weakest event among the strong La Niñas since 1982, although there were strong upwelling Kelvin wave activities. Moreover, compared with other strong La Niña events, the surface easterly wind anomalies and the warm pool extended further eastward in 2020/2021 La Niña, linking to a relatively weaker dipole-like pattern of the subsurface ocean temperature anomalies. The strength of all the strong La Niña events is determined by the in-phase amplification of all time scale variations. Their decay in the boreal spring and early summer is mainly controlled by the intra seasonal-inter seasonal variation. 2020/2021 La Niña was successfully predicted, however, the North American climate anomalies did not match the typical La Niña response, leading to low prediction skill in the extra-tropics during its mature phase.

1. Introduction

As the strongest interannual variability in the tropical oceans and the major source of predictability of global climate at seasonal-interannual time scales, El Niño–Southern Oscillation (ENSO) has been extensively studied in the last five decades since the pioneering work of Bjerknes (1969), and its global impact on climate variability and predictability has been well documented (Hu, Kumar, Jha, & Huang, 2020; McPhaden et al., 2021; National Research Council, 2010; Ropelewski & Halpert, 1987). As a result of these achievements, short-term (monthly-interannual) climate predictions are now operational at many climate service agencies with various dynamical and statistical approaches (Johnson et al., 2019; MacLachlan et al., 2015; O'Lenic et al., 2008). However, given the ENSO complexity and diversity (McPhaden et al., 2021; Timmermann et al., 2018), it is still a challenge to accurately forecast ENSO. For example, ENSO evolutions during 2010/2014 and 2017/2018 were not successfully predicted by the majority of ENSO prediction models (https://iri.columbia.edu/our-expertise/climate/enso/; Hu, Kumar, Huang, et al., 2020; Huang et al., 2017; Zhang et al., 2013; Zhu et al., 2016), putting forward the necessity of continuous studying the ENSO.

In the ENSO cycle, El Niño and La Niña represent two opposite phases and are driven by similar physical processes through the interaction among atmospheric circulation (wind and deep convection), surface and subsurface ocean fluctuations (e.g., Bjerknes, 1969; McPhaden et al., 2021). However, there are some asymmetric features in terms of their amplitude, zonal distribution pattern, meridional extent, zonal phase propagation, recharge-discharge process, and temporal evolution, as well as their global impact. To some extent, such asymmetric features imply the differences in the physics between the warm and cold phases (e.g., An et al., 2020; DiNezio et al., 2017; Hoerling et al., 1997; Iwakiri & Watanabe, 2020; Hu et al., 2014; Hu, Kumar, Huang, et al., 2017; Hu, Kumar, Zhu, et al., 2017; Huang et al., 2016; McPhaden & Zhang, 2009; Okumura et al., 2011, 2017; Timmermann et al., 2018; Zhang et al., 2009). One of the striking differences between El Niño and La Niña is the asymmetry of their temporal evolutions. El Niño normally lasts about 1 year from boreal summer to the following boreal spring, while La Niña mostly presents in consecutive multi-years (DiNezio et al., 2017; Hu et al., 2014; Okumura

et al., 2011). The frequent occurrence of second-year La Niña is a discrepancy from the cyclic behavior of the ENSO theory, such as the recharge and discharge oscillator (Jin, 1997a, 1997b; Hu, Kumar, Huang, et al., 2017; Yu & Fang, 2018).

Given the different features between El Niño and La Niña, it is necessary to examine not only the positive phase, but also the negative phase of the ENSO cycle. Moreover, due to irregular features, every event is unique. Thus, it is meaningful to examine and compare each event from a historical perspective. In 2020/2021, a La Niña was observed (Huang et al., 2021; L'Heureux et al., 2021). In this work, we examine the similarities and differences of the ocean and atmosphere anomalies between 2020/2021 and historical strong La Niña events. That includes sea surface temperature (SST), subsurface ocean temperature, atmospheric deep convection, and low-level wind anomalies in the tropical Pacific. Furthermore, through time scale decompositions of Niño3.4 SST anomaly (SSTA), the relative importance of different time scale components is identified during the evolutions of the various strong La Niña events since 1982. Last, the prediction of the La Niña event in 2020/2021 and the predictability of the extra-tropical climate during the mature phase of the La Niña event are verified.

The rest of the paper is organized as follows. The data and methods are introduced in Section 2. Section 3 shows the historical perspective of the evolution of oceanic and atmospheric anomalies in the equatorial Pacific during 2020/2021 La Niña and the differences compared with the historical strong La Niña events. Section 4 identifies the contributions of different time scale components to the strength and evolution of the strong La Niña events since 1982. Section 5 presents the real-time predictions of the La Niña event from a climate model and the unexpected impact on the North American region. A summary and discussion are given in Section 6.

2. Data and Methods

The data analyzed in this work are mainly from the Global Ocean Data Assimilation System on a $1° \times 1°$ grid (GODAS; Behringer, 2007). The GODAS is based on a quasi-global configuration of the Geophysical Fluid Dynamics Laboratory Modular Ocean Model version 3 (GFDL MOMv3) with a domain from 75°S to 65°N and has a resolution of 1° by 1° enhanced to 1/3° in the meridional direction within 10° of the equator. The model has 40 levels with a 10°m resolution in the upper 200 m. The model is forced by the momentum flux, heat flux, and freshwater flux from the National Centers for Environmental Prediction atmospheric reanalysis 2 (NCEP, R2) (Kanamitsu et al., 2002). The ocean temperature at the top model level is relaxed to weekly analyses of OIv2 SST (Reynolds et al., 2002) with a relaxation time-scale of 5 days, while the surface salinity is relaxed to its annual salinity climatology with a relaxation time-scale of 10 days. Both temperature and salinity profiles are assimilated in a 3DVAR scheme. Beginning from March 2007, altimetry sea level is assimilated.

To measure oceanic Kelvin wave activity along the equatorial Pacific, an oceanic Kelvin wave index was calculated using GODAS pentad (5°day) subsurface ocean temperature anomalies (OTAs). The index is defined as standardized projections of OTAs onto the first mode of an extended empirical orthogonal function (eEOF). The eEOF was driven for each 14 contiguous pentad OTAs of the upper 300 m along the equator between 135.5°E–94.5°W (Seo & Xue, 2005). The 14 patterns in the first eEOF mode represent 14 contiguous pentads and approximate the propagation of the Kelvin wave, which can be found at http://origin.cpc.ncep.noaa.gov/products/GODAS/ocean_briefing_new/eeve_1.gif. In this work, to eliminate the stationary component in the projection, 31-pentad running mean is removed and only the upwelling potion (negative index) is displayed to show the intensity of the upwelling Kelvin wave.

In addition to the Kelvin wave index, the oceanic variables analyzed in this work include monthly mean ocean temperature and monthly mean 20°C isotherm (D20) from GODAS. To examine the recharge/discharge processes associated with the equatorial Pacific Ocean heat exchange with the off-equator (Jin, 1997a, 1997b), the warm water volume (WWV) index is adopted which is defined as the D20 anomaly averaged in (5°S–5°N, 120°E–80°W) following Meinen and McPhaden (2000). Meanwhile, the WWV west and WWV east indices are also examined, which are defined as D20 anomaly averaged in the western and central (5°S–5°N, 120°E–155°W) and eastern (5°S–5°N, 155°W–80°W) tropical Pacific, respectively (Meinen & McPhaden, 2000).

The observation-based monthly mean SST is from OIv2 SST (Reynolds et al., 2002). Here, ENSO is defined based on both the Niño3.4 index and the relative Niño3.4 index. The Niño3.4 index is the SSTA averaged in (5°S−5°N, 170°W−120°W; the Niño3.4 region), while the relative Niño3.4 index is the Niño3.4 index minus

the SSTA averaged in the whole tropics (0°–360°, 20°S–20°N), to suppress the global warming signal following van Oldenborgh et al. (2021). The relative Niño3.4 index is renormalized to have the same variability as the original Niño3.4 series by multiplying by 1/(1−A) with "A" the regression of the 20°S–20°N SST anomalies on the Niño3.4 index as suggested by van Oldenborgh et al. (2021). One of the advantages of using the relative Niño3.4 index is that the interdecadal-trend components are largely suppressed in real-time, better representing the interseasonal-interannual time scale feature of ENSO.

In addition to analyzing the monthly mean surface wind stress and monthly mean geopotential height at 500 hPa (H500) from R2 (Kanamitsu et al., 2002), outgoing long-wave radiation (OLR) data on a 2.5° × 2.5° grid from Liebmann and Smith (1996) are used to measure the deep convection activities in the tropical Pacific. Observation-based precipitation analysis is from the monthly mean Climate Prediction Center (CPC) Merged Analysis of Precipitation on a 2.5° × 2.5° grid (CMAP; Xie & Arkin, 1997). Except for the OIv2 SST data from November 1981 to December 2021, all other observational-based data used in this work are from January 1979 to December 2021. All the anomalies are referred to as the departures from climatologies during January 1991–December 2020.

To identify the contributions of different time scales to the intensity and evolution of various strong La Niña events, Ensemble Empirical Mode Decomposition (EEMD) is adopted (Wu & Huang, 2009). Instead of using a priori "global" basis functions of rigid periods in Fourier transform-based time series analysis, EEMD is adaptive and derives optimal frequencies from the data itself, which provides a natural filter to separate components of different time scales (Huang et al., 1998; Huang & Wu, 2008).

We assess the real-time predictions of the La Niña in 2020/21 with initial conditions of January 2020–May 2021 and precipitation in December 2020–February 2021 (DJF 2020/21), which are from the NCEP Climate Forecast System version 2 (CFSv2; Saha et al., 2014; Xue et al., 2013). The 9-month predictions include 80 members within the last 20 days of each month and four forecasts per day with initial conditions from the Climate Forecast System Reanalysis (CFSR; Saha et al., 2010; Xue et al., 2011).

To show the possible influence of the La Niña on extra-tropical climate prediction, we adopt the official seasonal climate forecast verification of the NOAA CPC (https://www.cpc.ncep.noaa.gov/products/predictions/long_range/tools/briefing/seas_veri.grid.php). In the verification, the Heidke skill score (HSS) is used to measure how well a forecast relative to a randomly selected forecast, HSS = 100*(H-E)/(T-E), where "H" is the number of correct forecasts, "E" is the expected number of correct forecasts by luck, and "T" is the total number of forecasts. In the forecasts and observations, the seasonal average temperatures and total precipitation are classified into three categories—above average, below average, and near average. HSS > 0 means that the forecast is better than what would be expected by chance. HSS = 100 (−50) depicts a "perfect (worst)" forecast. HSS is computed for both all forecasts and "Non-CL" forecasts. "Non-CL" denotes forecasts with enhanced above or below normal chances. "Percent Coverage" is referred to the percent of the region with enhanced above or below chances forecast.

3. A Historical Perspective of the Evolution of 2020/2021 La Niña

The negative SSTAs were initiated in April 2020 and accompanied by a strong upwelling Kelvin wave represented by negative D20 anomalies (Figure 1a). The negative SSTAs weakened slightly in June 2020 after the upwelling Kelvin wave reached the South American coast. Then, the negative SSTAs re-strengthened and reached their peak in October-December 2020 in association with strong atmosphere-ocean coupling (L'Heureux et al., 2021). In consistence with the SSTA pattern (warming in the western and cooling in the eastern equatorial Pacific), convection was suppressed in the central tropical Pacific, and low-level easterly wind anomalies prevailed in the equatorial Pacific since July 2020 (Figure 1b), in agreement with the ENSO theory of the atmosphere-ocean coupling (Bjerknes, 1969). The La Niña event ended in May 2021 with the emergence of positive D20 anomalies (contours in Figure 1a) and small OLR anomalies (shading in Figure 1b), implying a decoupling between the atmosphere and ocean, although the relative Niño3.4 index is still cooler than −0.5°C with the value of −0.52°C in May 2021 (Figure 2a).

Historically, there are six-strong La Niña events with the peak values of the relative Niño3.4 index ≤ −1.5°C during 1982–2021: 1988/1989, 1998/1999, 1999/2000, 2007/2008, 2010/2011, and 2020/2021 (Figure 2a). The
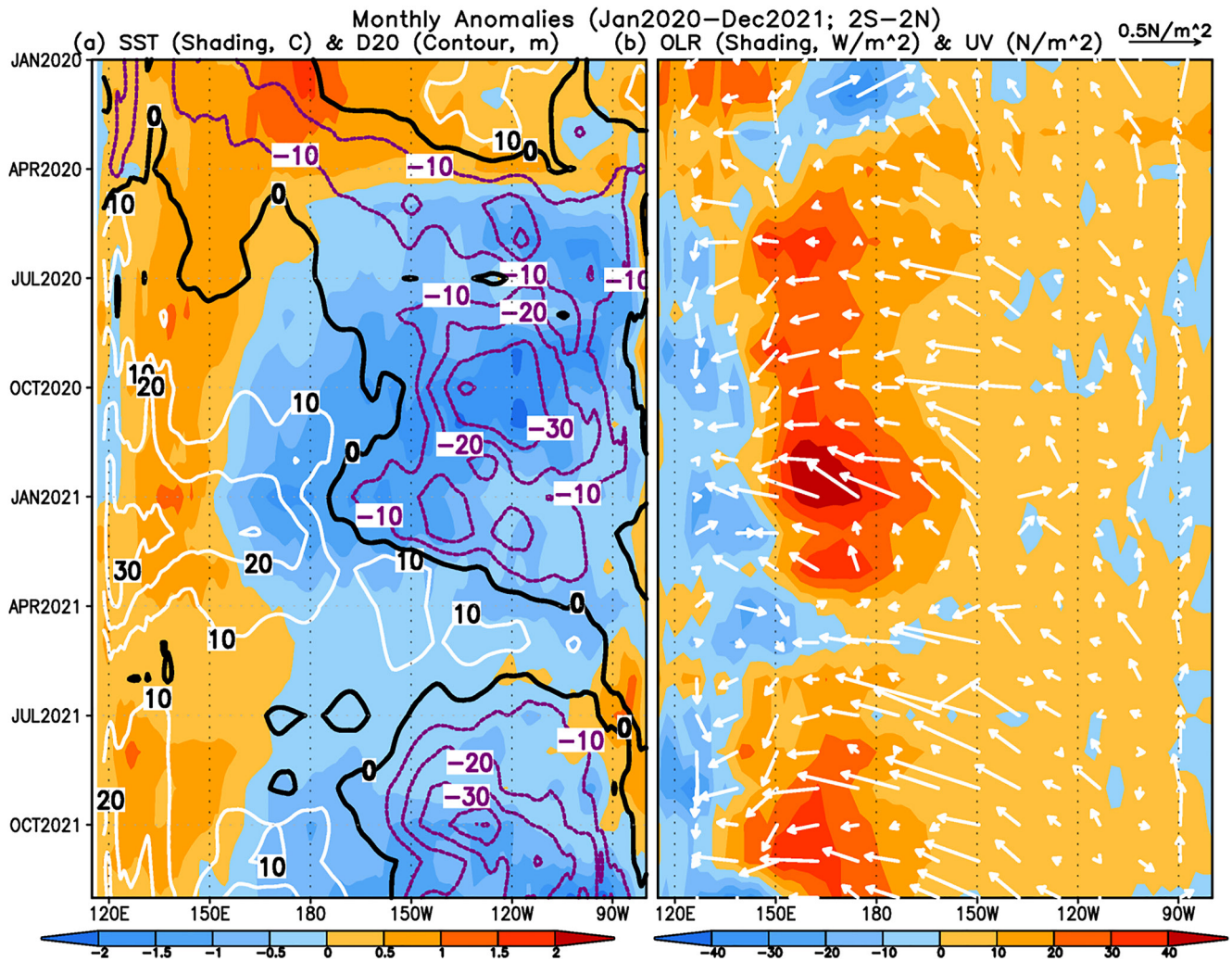
Figure 1. Hovmöller diagrams of the monthly mean of (a) sea surface temperature (SST) (shading) and D20 (contours) anomalies, and (b) outgoing long-wave radiation (OLR) (shading) and surface wind stress (vector) anomalies averaged in 2°S–2°N during (a) January 2020-December 2021. The units are °C for SST, m for D20, W/m² for OLR, and N/m² for wind stress.

peak values of the relative Niño3.4 index are −2.32°C in November 1988, −1.93°C in December 1998, −1.84°C in January 2000, −1.98°C in February 2008, −1.84°C in September 2010, and −1.77°C in October 2020, respectively. From the historical perspective, 2020/2021 La Niña ranks sixth in the strength based on the monthly mean relative Niño3.4 index and is the weakest strong La Niña event since 1982. Nevertheless, we should point out that for La Niña or El Niño strength ranking, the maximum SSTA in the tropical central and eastern Pacific may present in slightly different months and locations in various events, and it is also affected by the uncertainties/biases in the SST data, which may affect the strength ranking to some extent (e.g., Huang et al., 2013, 2016).

The predictability of the ENSO cycle derives from deterministic wind-driven ocean dynamics that govern the slowly evolving heat content of the upper ocean (Hu, Kumar, Zhu, et al., 2017; Latif et al., 1998; Meinen & McPhaden, 2000). According to the recharge and discharge paradigm (Jin, 1997a, 1997b), the oscillation between cold and warm phases, or the cyclic feature of ENSO evolution links to the ocean heat exchange between the equator and off-equator in the Pacific. During an El Niño decay phase, the equatorial Pacific losses heat to the off-equatorial Pacific, while during a La Niña decay phase, the equatorial Pacific gains heat from the off-equatorial Pacific, leading to the ENSO phase transition and the cyclic feature of the ENSO cycle. Such a phase transition is shown as the clockwise evolution in the phase orbit diagram of the Niño3.4 and WWV indices (Figure 3; e.g., Chen et al., 2015; Hu, Kumar, Zhu, et al., 2017; Hu, Kumar, Jha, & Huang, 2020; Hu, Kumar, Huang, et al., 2020; Kessler, 2002; Li et al., 2020; McPhaden, 2012; Meinen & McPhaden, 2000). From Figure 3,
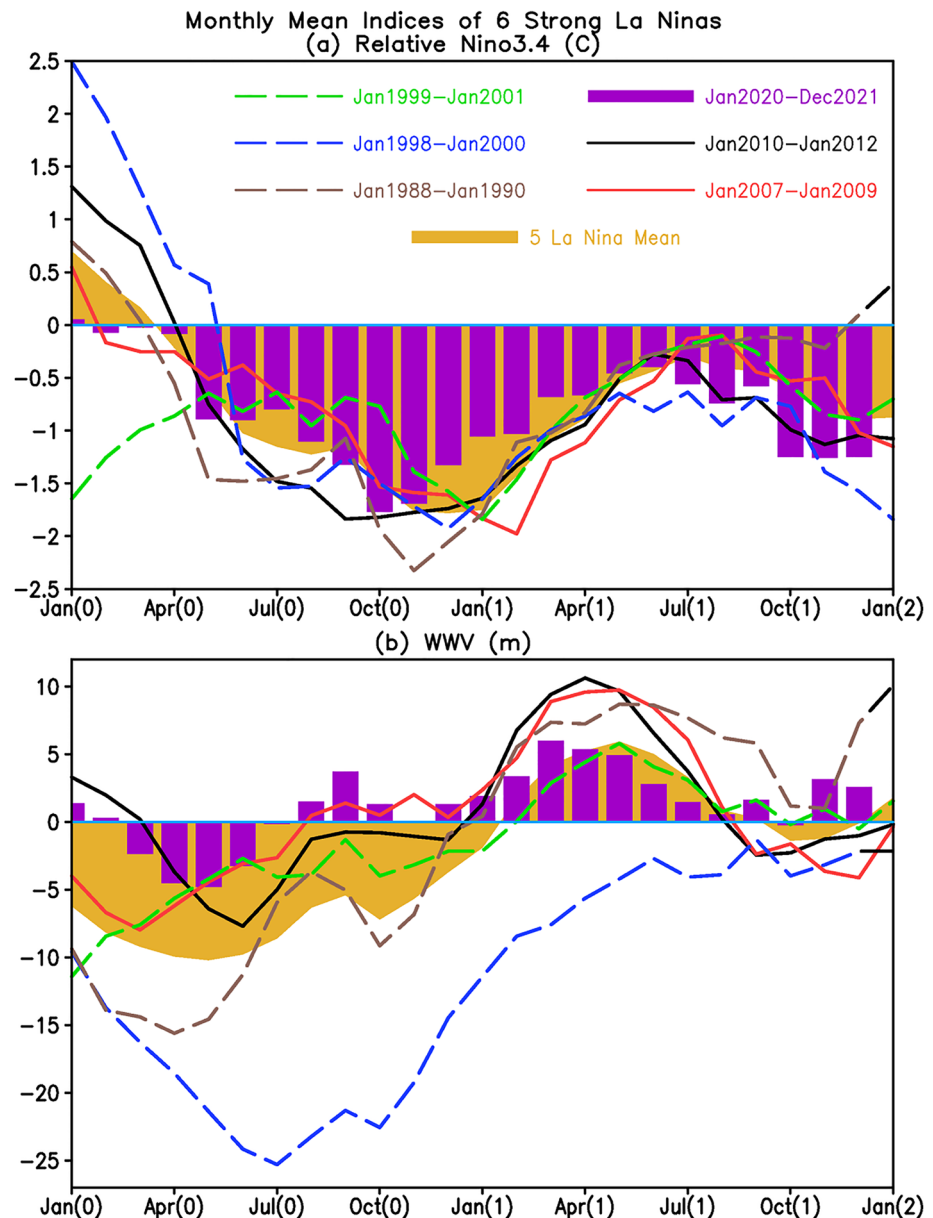
Figure 2. Time evolution of the monthly mean (a) relative Niño3.4 and (b) warm water volume indices during six-strong La Niña events: January 1988–January 1990 (brown dash line), January 1998–January 2000 (blue dash line), January 1999–January 2001 (green dash line), January 2007–January 2009 (red solid line), January 2010–January 2012 (black solid line), and January 2020–December 2021 (purple bars). The shading represents the average of the first five events. The unit is °C for (a) and m for (b).

it is seen that the clockwise evolution is evident in 1988/1989, 1998/1999, 2007/2008, and 2010/2011 La Niña events, while it is ambiguous in the 1999/2000 and 2020/2021 events. That is consistent with the fact that among the six-strong La Niñas, except for that 1999/2000 La Niña event was a continuation of 1998/1999 La Niña event and 2020/2021 La Niña is a unique event which developed from a "neutral" condition of ENSO (borderline El Niño), the other four events are rebounded from El Niño events consisting with the cyclic feature of the ENSO cycle (Figure 2). For a longer historical comparison, in a recent ENSO blog, Dr. Emily Becker noted that among the 12 La Niña events since 1950, the La Niña in 2020/21 is the only one that did not follow a full-blown El Niño (https://www.climate.gov/news-features/blogs/enso/december-2021-la-ni%C3%B1a-update-visual-aids).   Thus, since 2020/2021 La Niña was uniquely followed by a borderline El Niño instead of an El Niño, the equatorial-heat discharge was the weakest among the strong La Niñas since 1982 (Figure 2b), resulting in a relatively weaker
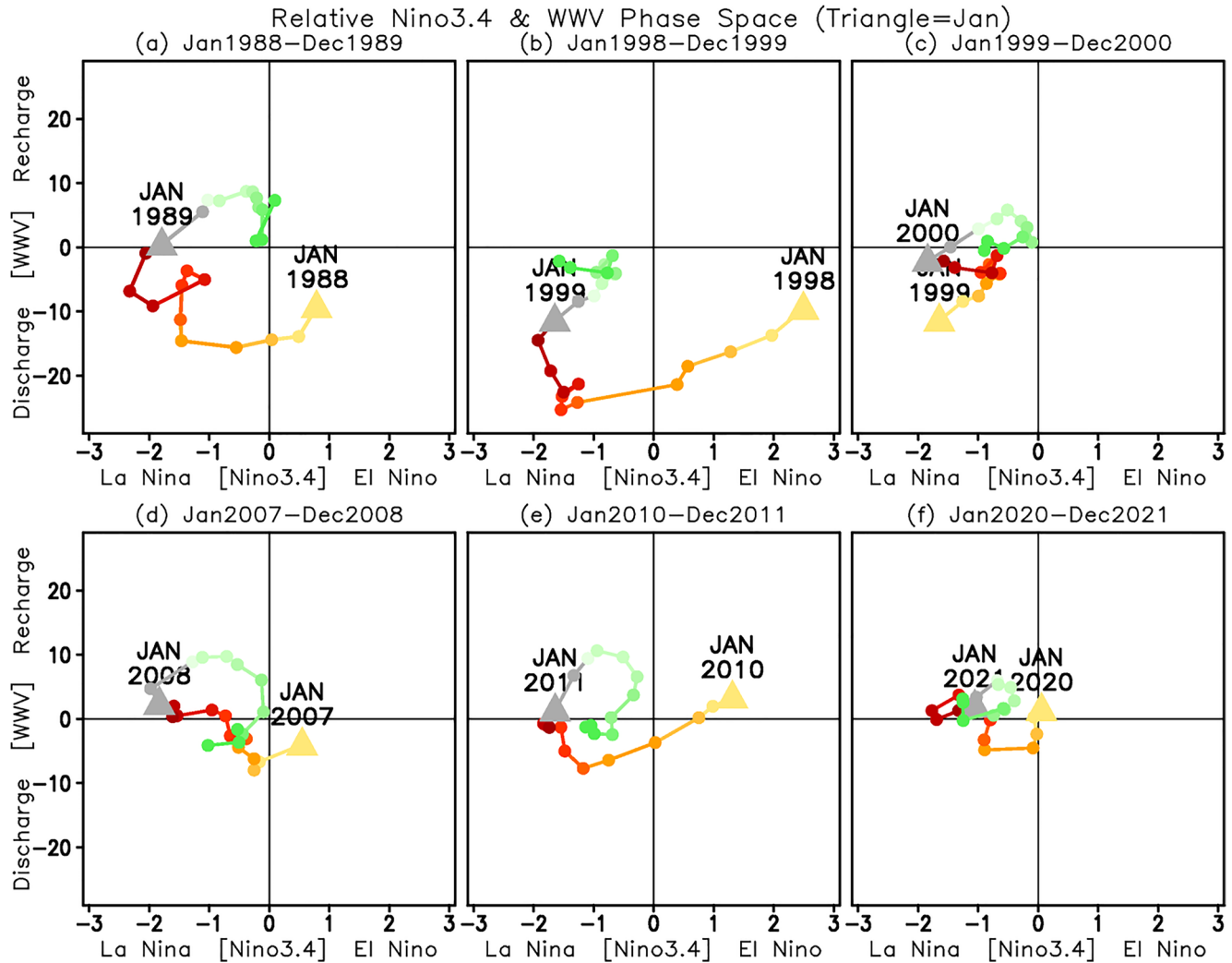
Figure 3. Phase orbits of the monthly mean relative Niño3.4 (x-axis; °C) and warm water volume (y-axis; m) indices during (a) January 1988–December 1989, (b) January 1998–December 1999, (c) January 1999–December 2000, (d) January 2007–December 2008, (e) January 2010–December 2011, and (f) January 2020–December 2021. The triangle marks represent January and different colors represent different months.

event (Latif et al., 1998; Meinen & McPhaden, 2000), although the overall upwelling Kelvin wave was relatively strong during its development phase (Figure 4). That implies the importance of the recharge/discharge processes in determining the ENSO strength (e.g., Meinen & McPhaden, 2000). In addition to the trade wind anomaly, the opposite variation of WWVwest and WWVeast indices (orange and purple curves, Figure 5) may be a factor resulting in the strong negative values of the Kelvin index in 2020/2021 La Niña.

Interestingly, accompanied by the overall small WWV index during 2020/2021 La Niña event, the contrast of the subsurface OTAs between the western and eastern equatorial Pacific, which are referred to as WWVwest and WWVeast indices, respectively, enlarged since July 2020 (orange and purple lines, Figure 5f). That implies a strengthening of the so-called tilt or dipole mode of the subsurface ocean temperature variability along the equatorial Pacific which is measured by WWVeast - WWVwest (shading in Figure 5f). Statistically, the tilt mode varies in phase with the ENSO cycle (e.g., Clarke, 2010; Kumar & Hu, 2014). Such opposite variations of the thermocline in the western and eastern equatorial Pacific are also evident in the other five-strong La Niña events (Figures 5a–5e). The opposite thermocline fluctuations along the equatorial Pacific with positive anomalies in the west and negative anomalies in the east (i.e., enlarged thermocline slop; shading in Figure 5) are linked to easterly wind anomaly at the ocean surface (bars in Figure 5). Physically, the zonal distribution pattern of the subsurface ocean temperature anomaly is in balance with the surface zonal wind anomalies (Jin, 1997a, 1997b;
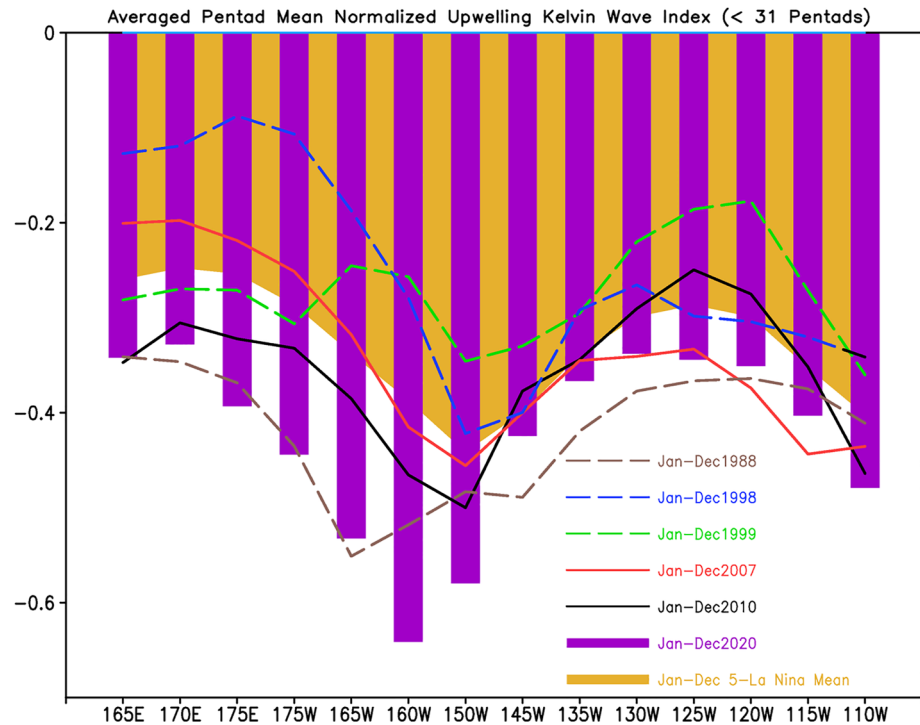
Figure 4. Longitude-dependent *negative* pentad oceanic Kelvin wave index averaged in January–December during the development years of the six-strong La Niña events: 1988 (brown dash line), 1998 (blue dash line), 1999 (green dash line), 2007 (red solid line), 2010 (black solid line), and 2020 (purple bars). The shading represents the average of the first five events. To eliminate the stationary component, the 31-pentad running mean is removed.

Clarke, 2010; Kumar & Hu, 2014). Moreover, the zonal wind anomalies link to the ENSO strength and diversity (e.g., Chen et al., 2015; Harrison & Vecchi, 1997; Hu et al., 2012; Hu & Fedorov, 2016).

The zonal contrast of the subsurface ocean condition is associated with the zonal displacement of the warm pool eastern edge, which has been used to examine the development of El Niño events (e.g., Picaut, et al., 1996; Clarke & Gorder, 2001). Here, we show the zonal displacement of the warm pool eastern edge connected with the development of the La Niña events. Compared with the other five-strong La Niña events, the warm pool eastern edge (or the cold tongue westward extension) variation measured by the 28°C isotherm (T28) of SST along the equatorial Pacific did extend further eastward in 2020/2021 La Niña (Figure 6a). That is consistent with the longitudinal extension of the surface easterly wind anomalies (not shown) as well as the relatively strong upwelling Kelvin wave (Figure 4). Compared with the five-strong La Niña events, the longitude of T28 during the 2020/2021 La Niña event was mostly in the easternmost location during June-December 2020 (Figure 6a). Such eastward displacement of the warm pool and surface easterly wind anomalies seems to play a role in the strength of the dipole-like pattern of the subsurface OTAs with cooling in the eastern Pacific and warming in the western Pacific (Figures 5, 6a, 7).

Statistically, a larger negative dipole index of the thermocline fluctuation (WWVeast–WWVwest) is associated with a further westward location of the warm pool (or cool tongue) for all month data during January 1979-December 2021 (green dots in Figure 6b). That may imply that compared with the other five-strong La Niña, the eastward extension of the location of the warm pool and the easterly wind anomaly is associated with the relatively smaller negative dipole index (shading in Figure 5). That may be a factor leading to a relatively weaker La Niña event in 2020/2021. Interestingly, whether there is a linear relationship between the cold-tongue westward extension and the intensity of the dipole mode depends on the cold-tongue westward extension. When the longitude location of T28 is located west of 170°W, the linear relationship holds roughly, but when it is located east of 170°W, there is no linear relationship due to the very shallow thermocline climatologically. Also, the linear relationship does not hold for the positive dipole index (red dots in Figure 6b). Such asymmetry deserves further investigation.
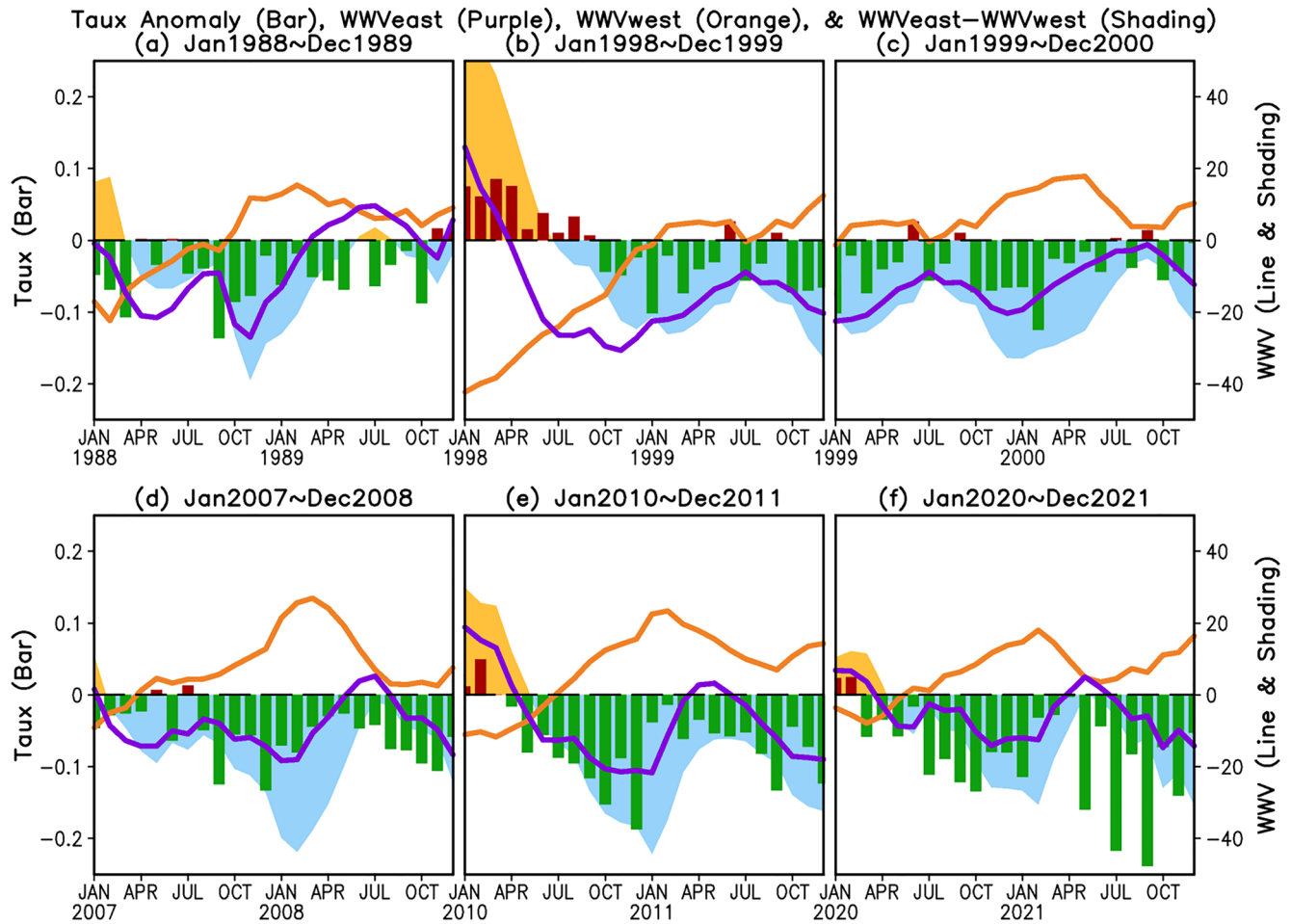
Figure 5. Time evolution of the monthly mean of the zonally averaged zonal wind stress anomaly (bar), warm water volume (WWV) east (purple line), WWV west (orange line), and WWVeast-WWVwest (shading) indices during (a) January 1988–December 1989, (b) January 1998–December 1999, (c) January 1999–December 2000, (d) January 2007–December 2008, (e) January 2010–December 2011, and (f) January 2020–December 2021. The zonally averaged zonal wind stress anomaly is the mean in 5°S–5°N, 120°E–80°W. The unit is N/m² for the zonal wind stress and m for the WWVeast, WWVwest, and WWVeast-WWVwest indices.

The dipole-like pattern of the thermocline fluctuation along the equatorial Pacific is dominated and amplified in boreal autumn and winter during all the six-strong La Niña events (Figure 7). However, the dipole-like pattern might be interrupted by a downwelling Kelvin wave or down welling Kelvin wave-like disturbances. For example, during the La Niña in 1988/89 (Figure 7a), two strong downwelling Kelvin waves initiated in October 1988 and 1989, respectively, push warm water eastward, which hindered the occurrence of the second-year La Niña (Figure 2a), as indicated by Hu et al. (2014). Compared with that in 1988/89 La Niña event, down welling Kelvin wave-like disturbances are also present but much weaker in the other four-strong La Niña events that are followed by second-year La Niñas (Figures 2a, 7b–7e). As we know that the Kelvin wave was triggered by surface westerly or easterly wind burst event (e.g., Harrison & Vecchi, 1997; Hu et al., 2012; Hu & Fedorov, 2016) which is largely a weather noise and unpredictable beyond the subseasonal time scale, the crucial role of the Kelvin wave activity in the thermocline disturbance and ENSO evolution points to a limitation of ENSO predictability (Hu et al., 2019). The duration of La Niña events may be affected by the amplitudes of preceding El Niño events through the recharge process of the equatorial oceanic heat content (Wu et al., 2019). Two-year La Niña events are mostly preceded by a strong El Niño, thus they are predictable to some extent (Wu et al., 2021). However, 2019/2020 is not an El Niño, 2020/2021 seems to be followed by a second-year La Niña event in 2021/2022 That may imply that in addition to the precedent recharge and discharge process, there are some other mechanisms controlling the duration.
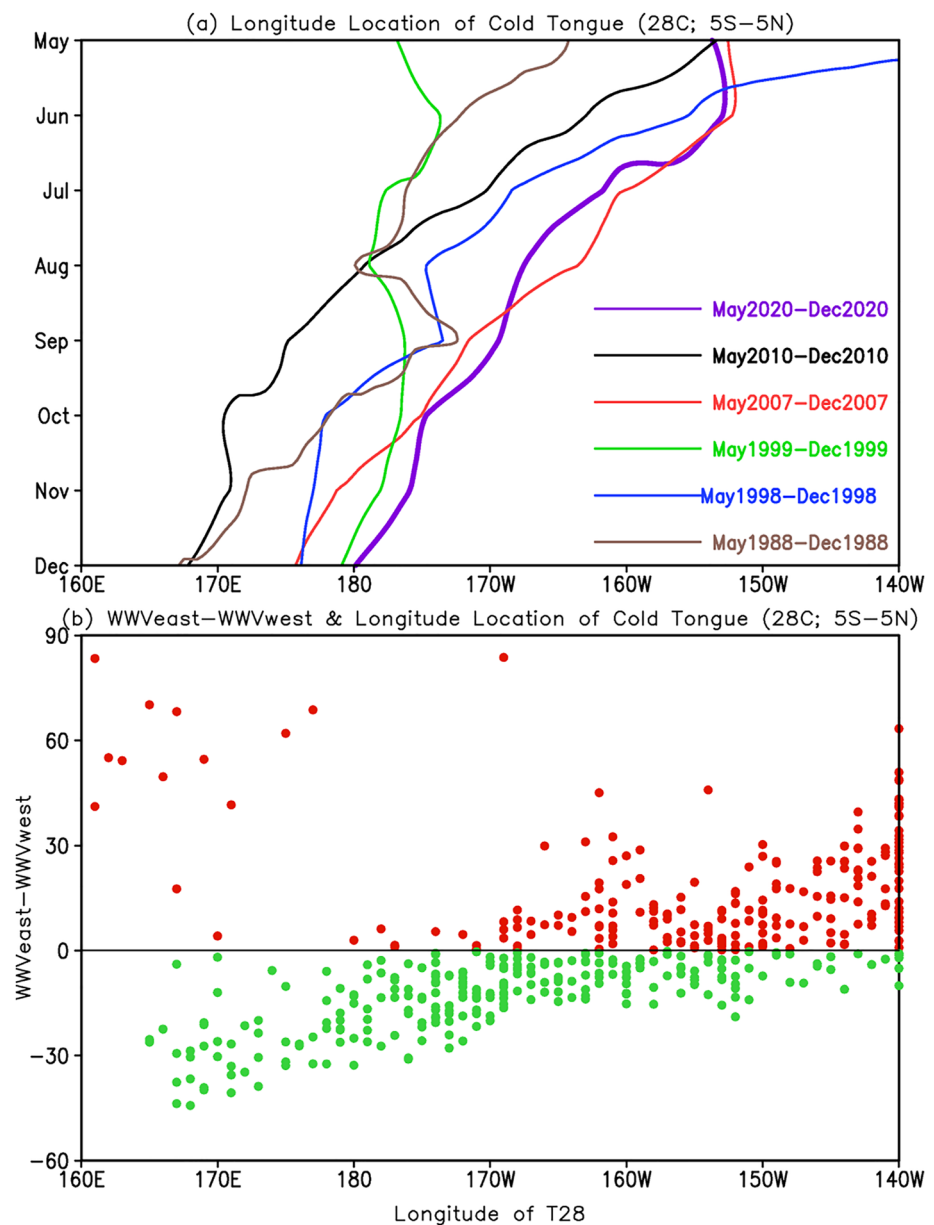
Figure 6. (a) Temporal evolution of the longitude locations of 28°C isotherm of the monthly mean sea surface temperature (SST) (T28) averaged in 5°S–5°N during May-December 1988 (gray), 1998 (blue), 1999 (green), 2007 (red), 2010 (black), and 2020 (purple); (b) scatter plot between WWVeast-WWVwest (y-axis) and the longitude locations of T28 averaged in 5°S–5°N (x-axis) during January 1979–December 2021.

4. Contribution of Different Time Scale Variations to the Strength and Evolution of the Strong La Niñas

Although ENSO is an interseasonal-interannual phenomenon, lower-frequency variations do influence the evolution and intensity of ENSO (e.g., Li et al., 2019; Yeo et al., 2016). For example, intraseasonal-interseasonal and interannual components have a positive contribution to the strengths of all strong El Niño events during 1979–2017, however, the contribution of the interdecadal-trend time scale component is varied with events: it is negligible during 1982/1983 El Niño, negative during 1997/1998 El Niño, and positive during 1991/1992 and 2015/2016 El Niños (Li et al., 2019). Similar to Li et al. (2019), to identify contributions of different time scale variations to La Niña strength and evolution, EEMD is applied to the Niño3.4 index instead of the relative Niño3.4 index to maintain the variations of all time scales. Figure 8 displays the raw Niño3.4 index (shading),
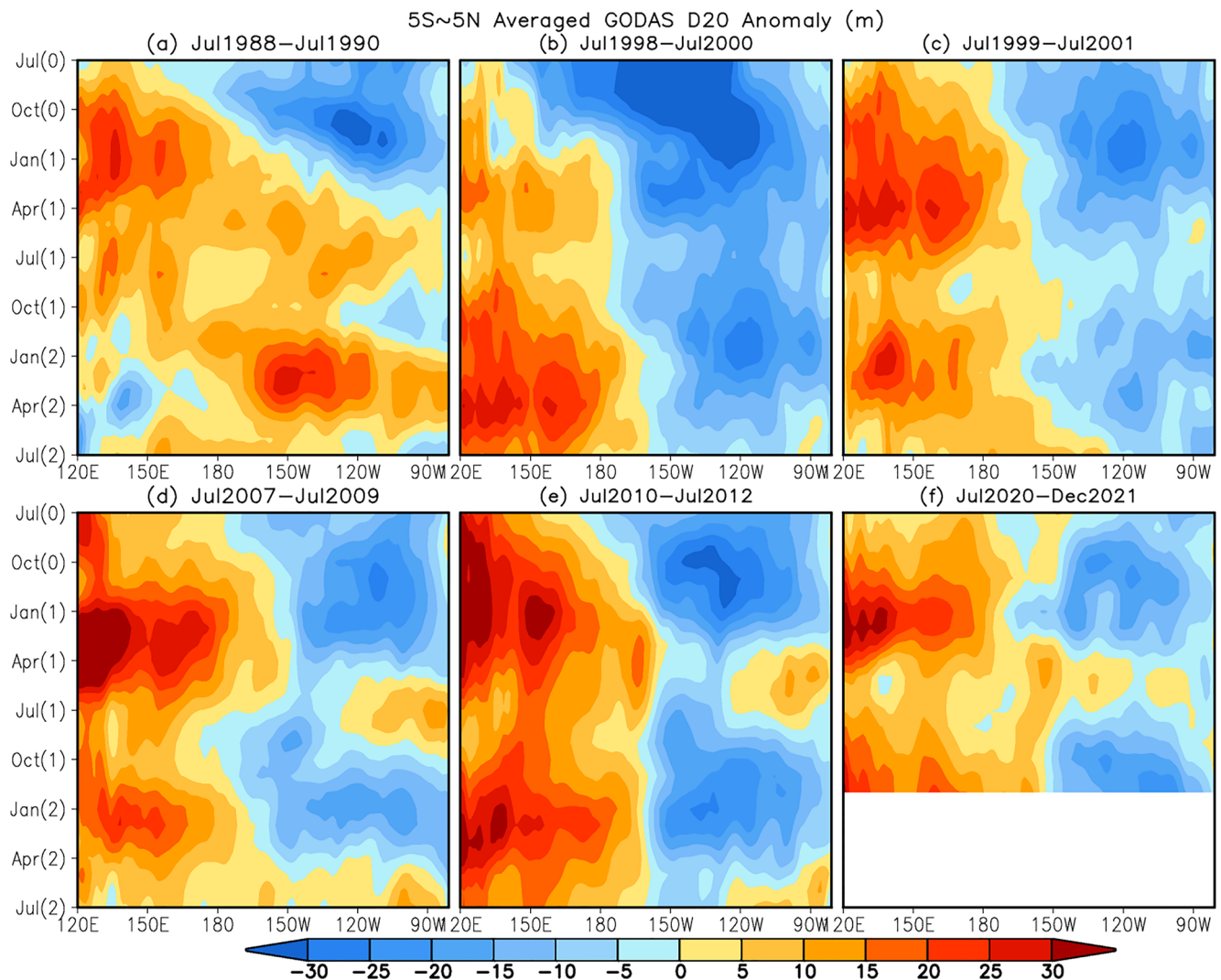
Figure 7. Hovmöller diagrams of the monthly mean of D20 anomalies averaged in 5°S–5°N during (a) July 1988–July 1990, (b) July 1998–July 2000, (c) July 1999–July 2001, (d) July 2007–July 2009, (e) July 2010–July 2012, and (d) July 2020–December 2021. The unit is m.

its components at intraseasonal-interseasonal (black dot lines; time scales shorter than 1 year), interannual (red solid lines; time scales between 1 and 10 years), and interdecadal-trend (green dash lines; time scales longer than 10 years) time scales in the six-strong La Niña events since 1982. The EEMD results are similar to that using a time-scale filter (not shown), suggesting the robustness of the EEMD results.

Consistent with the strong El Niño events (Li et al., 2019), the interannual components are negative in the six La Niña events, meaning a positive contribution to the strengths of all the strong La Niña events (Figure 8). More-over, the intraseasonal-interseasonal components are also negative in the peaks of all the La Niña events (black dot lines, Figure 8). Interestingly, the interdecadal-trend components (green dish lines, Figure 8) also enhanced the intensity of all the La Niña events, but the amplitudes are weaker than those of the interannual and intrasea-sonal-interseasonal components. In the observations (not shown; also L'Heureux et al., 2013), there is almost no linear trend in the Niño3.4 region during January 1982-December 2021. Nevertheless, it cannot be ruled out that the negative values of the interdecadal-trend component during all the La Niña events might be partially due to the EEMD projection of higher frequency components on it. Thus, the strengths of the strong La Niña events are the results of the in-phase amplification of the intraseasonal-interseasonal, interannual, and interdecadal-trend components.
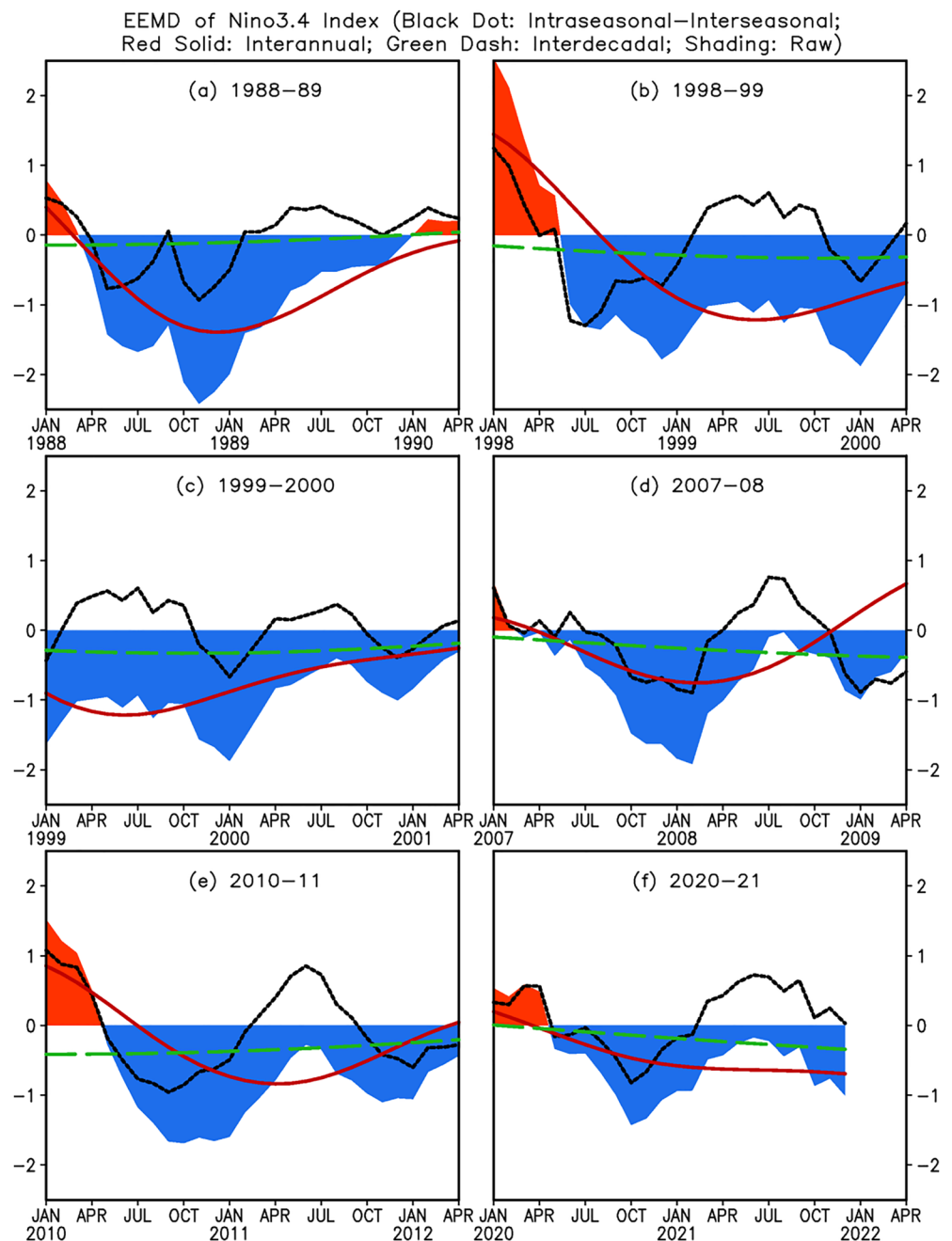
Figure 8. Monthly mean Niño3.4 index during (a) January 1988–April 1990, (b) January 1998–April 2000, (c) January 1999–April 2001, (d) January 2007–April 2009, (e) January 2010–April 2012, and (f) January 2020–December 2021. The shading, black dot, red solid, and green dash lines represent raw data, Ensemble Empirical Mode Decomposition components at intraseasonal-interseasonal, interannual, and interdecadal and longer time scales, respectively. The unit is °C.

Contrasting to the strong El Niño events, the contributions of the intraseasonal-interseasonal component vary in the different events and different times during the La Niña events. Specifically, during boreal spring and early summer, the intraseasonal-interseasonal components are positive in all the La Niña events. Physically, the interannual component directly links to the recharge/discharge oscillator, while the intraseasonal-interseasonal component may be associated with the atmosphere-ocean coupling as well as the influence of the extratropical atmospheric disturbances (e.g., Chen et al., 2018, 2020; Tseng et al., 2017). For example, Chen et al. (2015) argued that during a mature phase of a La Niña, the enhanced easterly wind anomalies consistently induce a

transport convergence of the Pacific Subtropical Cells, which leads to increasing WWV within a few months, affecting the phase transition of the ENSO cycle. In fact, both the recharge/discharge oscillator, measured by the WWV index, and ENSO strength, measured by the Niño3.4 index, are an integration of all the time scales and mainly determined by the combination of the interannual and intraseasonal-interseasonal components. For example, when the interannual and intraseasonal-interseasonal components are in phase, such as 1988/89 (Figure 8a), the La Niña is strong, and it is weak when they are not in phase, such as in 2020/21 (Figure 8f).

Therefore, the peaks (or strengths) of the strong La Niña events are determined by the in-phase amplification of the intraseasonal-interseasonal, interannual, and interdecadal-trend variations. Although both the interannual and intraseasonal-interseasonal variations contribute to the decay of La Niñas (Figure 8), the phase change of the intraseasonal-interseasonal variation precedes that of the interannual variation, thus, the decay of the strong La Niña events in the boreal spring and early summer is mainly controlled by the intraseasonal-interseasonal variation.

5. Predictions and the Impacts

The La Niña event in 2020/2021 was successfully predicted by CFSv2 with the initial conditions (ICs) from January–September 2020 (Figures 9b–9e) (May-November 2020; contours in Figure 10), despite some biases in predicting the cooling strength. For example, although the model with ICs in January 2020 predicted a cooling tendency, the cooling amplitude was underestimated (Figure 9a). This large bias might be due to the spring predictability barrier (Xue et al., 2013). The cooling amplitude was overestimated in the forecasts with ICs in November 2020 (Figure 9f). The overall successful predictions are consistent with statistical-high prediction skills of ENSO of CFSv2 (Saha et al., 2014; Xue et al., 2013). For the forecasts with ICs in March-May 2021 (Fig. 9h, j), a second-year La Niña (or borderline La Niña) was predicted. That is consistent with the historical perspective: all strong La Niñas since 1979 were followed by a second-year La Niña unless a strong down welling Kelvin wave presented (Hu et al., 2014).

For the precipitation anomalies in DJF 2020/21, CFSv2 consistently predicted a La Niña-like pattern in the tropical Pacific with negative SSTAs in the central and eastern Pacific with ICs in May-November 2020 (Figure 10). For the North American region, except for mostly below normal precipitation predicted with ICs in November 2020 (shading in Figure 10a), the predictions with ICs in September, July, and May 2020 call a typical La Niña-like pattern with above normal in the northern tier and below normal in the southern tier. However, that has few similarities with the observations (shading in Figure 11a), meaning an unsuccessful prediction for the precipitation in North America in DJF 2020/2021.

In an NOAA ENSO blog post, Dr. Johnson pointed out that there was an unusual mismatch between the typical La Niña atmospheric circulation pattern and the observed one in December 2020-January 2021 over North America (https://www.climate.gov/news-features/blogs/enso/did-northern-hemisphere-get-memo-years-la-ni%C3%B1a). Consistent with Dr. Johnson's argument, there are few similarities for the spatial distribution of both the precipitation and H500 anomalies over the North American sector. Geographically, the observed and reconstructed precipitation anomalies in DJF 2020/21 are opposite mainly in the northern tier of the North American continent, and they are similar in the southern tier. As a result, for the North American region (30°–48°N, 75°–125°W), the pattern correlation is 0.03 between the observed and reconstructed precipitation and −0.08 between the observed and reconstructed H500. We can see from Figure 11b that the reconstructed pattern based on the statistical relationship is very weak, and that indicates the diversity of the influences of the historical La Niña events. Therefore, it is not surprising that a single case does not match the statistical results of multiple cases.

The mismatch between the observed and model-predicted (or La Niña's historical perspective) anomalies in the North American region losses the ground for successful seasonal climate forecasts in the U. S. That is reflected in the official seasonal climate forecasts of NOAA CPC, since ENSO is a key predictor in its official seasonal climate forecasts (O'Lenic et al., 2008; Peng et al., 2013). For the official forecast of precipitation over the U. S. in DJF 2020/21, HSS is −0.29 for non-equal chance (non-EC) forecasts and −0.22 for all forecasts (Table 1). The corresponding HSS for the temperature forecasts is −22.35 and −17.24 (Table 1; https://www.cpc.ncep.noaa.gov/products/predictions/long_range/tools/briefing/seas_veri.grid.php). The unsuccessful forecasts may imply that the ENSO-relevant portion was overshadowed by the internal dynamic or/and other processes (such as land
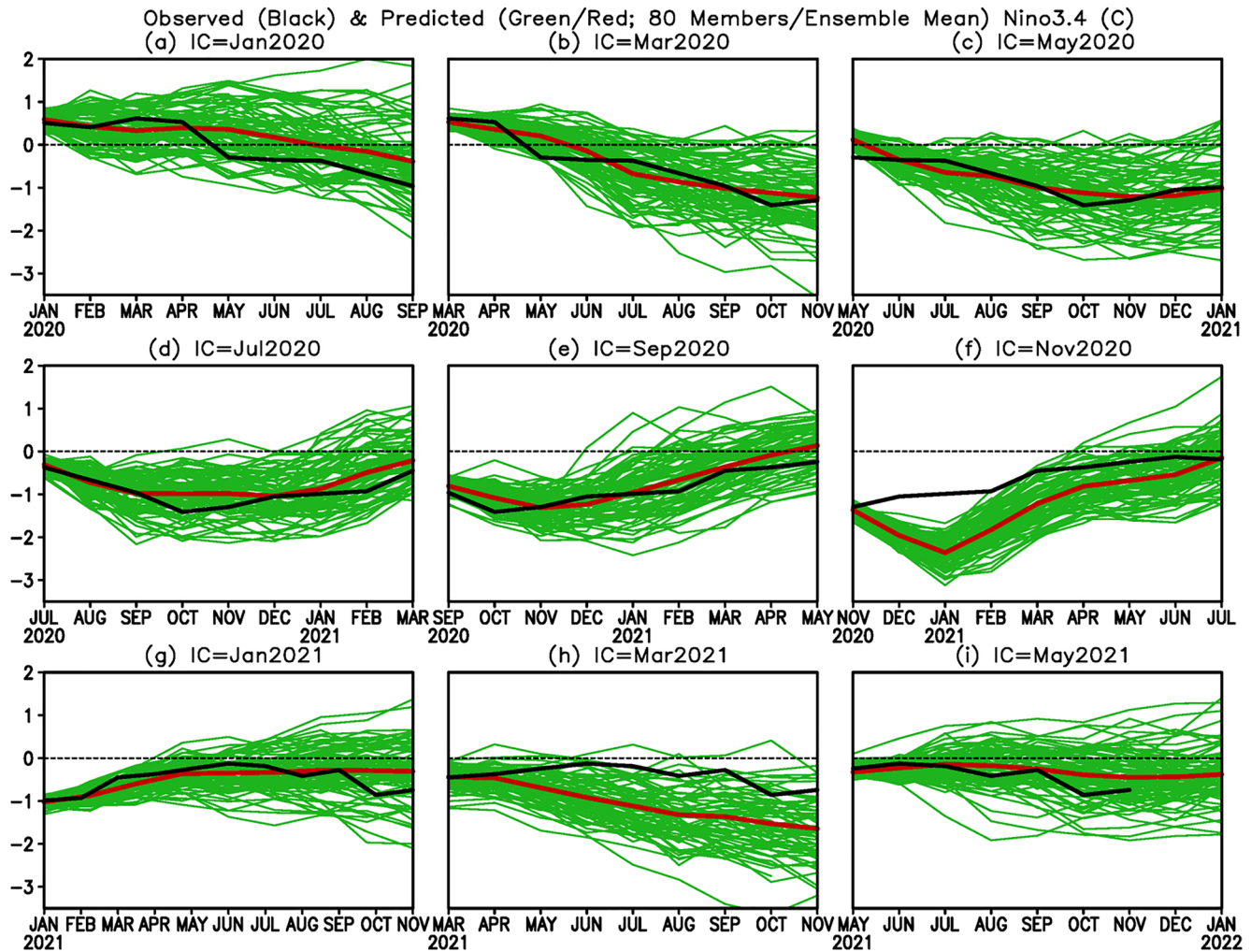
Figure 9. Observed (black line) and Climate Forecast System version 2 (CFSv2) predicted monthly mean Niño3.4 index with initial conditions in (a) January 2020, (b) March 2020, (c) May 2020, (d) July 2020, (e) November 2020, (f) November 2020, (g) January 2021, (h) March 2021, and (i) May 2021. The green lines denote the 80 individual members, and the red line represents the ensemble mean of 80 members. The unit is °C.

surface process, sea ice, and stratosphere; National Research Council, 2010) driven anomalies, leading to the low predictability in DJF 2020/21.

6. Summary and Discussion

ENSO is the strongest interannual variability in the tropical Pacific and the major source of global climate predictability. Both cold and warm phases of ENSO can cause global climate disasters. Nevertheless, each event is unique in its evolution, associated physics, and impacts. In this work, we examined the evolution of oceanic and atmospheric anomalies in the equatorial Pacific during 2020/2021 La Niña, compared with the historically strong La Niña events, identified the contributions of different time scale components to the strength and evolution of the La Niña events, and assessed the predictions of 2020/2021 La Niña event from a climate model and the unexpected impact in the North American region.

2020/2021 La Niña emerged in August 2020 and dissipated in May 2021 with a peak relative Niño3.4 value of −1.77°C in October 2020. The SSTA pattern with warming in the western and cooling in the eastern equatorial Pacific, suppressed convection in the central tropical Pacific, and prevailed easterly low-level wind anomalies in the equatorial Pacific during August 2020–May 2021 are in line with the theory of the atmosphere-ocean coupling associated with ENSO (Bjerknes, 1969). From the historical perspective, the strength of 2020/2021 La
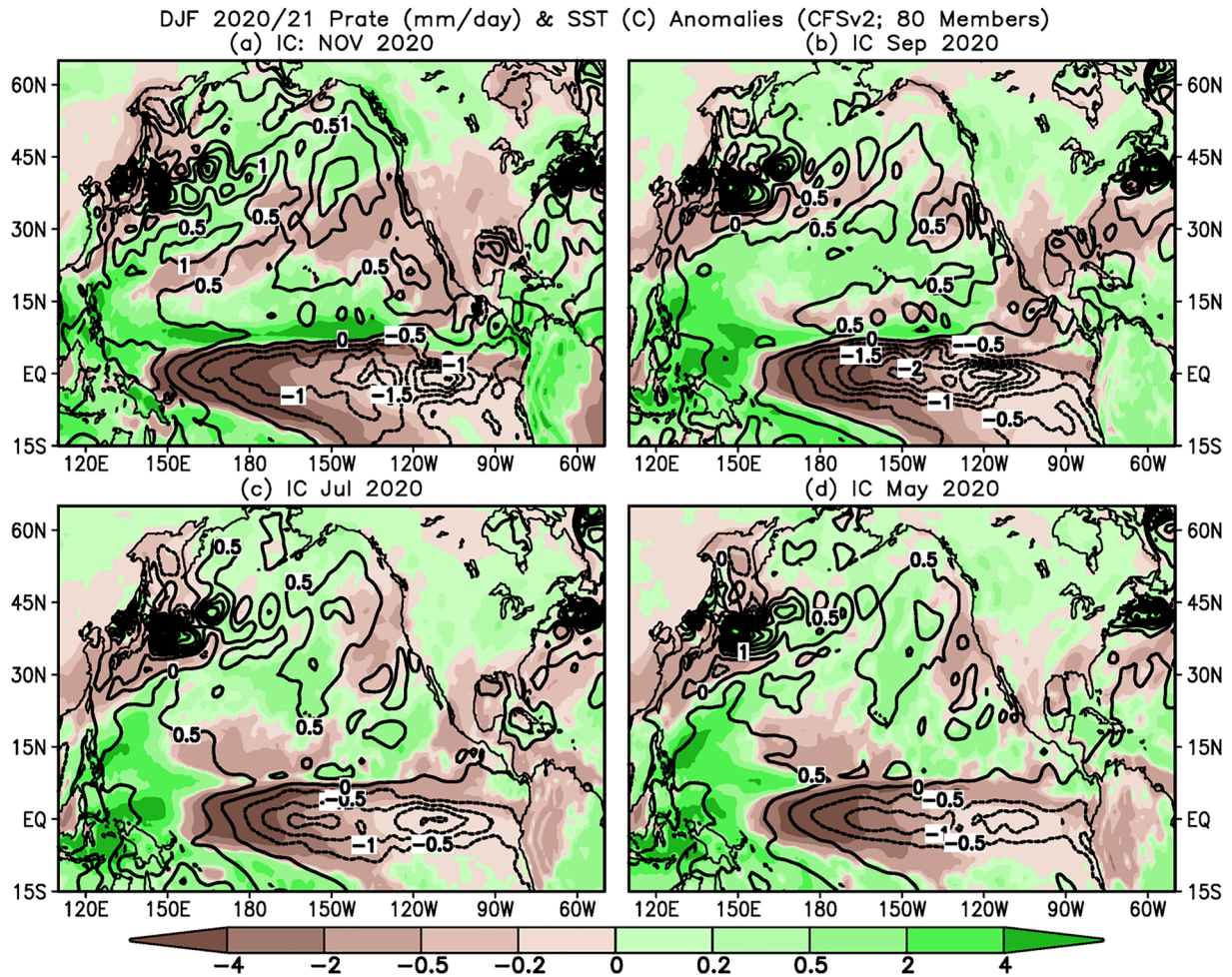
Figure 10. Climate Forecast System version 2 (CFSv2) predicted precipitation (shading) and subsurface ocean temperature (SST) (contour) anomalies in DJF 2020/21 with initial conditions in (a) November 2020, (b) September 2020, (c) July 2020, and (d) May 2020. The forecasts are the ensemble mean of 80 members. The unit is mm/day for precipitation and the contour interval of SSTA is 0.5°C.

Niña ranks sixth based on the relative Niño3.4 index since 1982. 2020/2021 La Niña was uniquely preceded by a borderline El Niño instead of an El Niño, thus the equatorial-heat discharge process was weak. That resulted in a relatively weaker event among the strong La Niñas since 1982, although the overall upwelling Kelvin wave was relatively strong during the development phase of 2020/2021 La Niña. Accompanied by the overall small WWV index, a strong tilt or dipole mode of the subsurface OTAs presents along the equatorial Pacific with positive in the west and negative in the east. Compared with the five-strong La Niña events since 1982, the surface easterly wind anomalies and the warm pool presented further eastward. That may be associated with the relatively weaker dipole-like pattern of the subsurface OTAs along the equatorial Pacific.

The peak values of the La Niña events are determined by the in-phase amplification of the intraseasonal-interseasonal, interannual, and interdecadal-trend variations. That is in contrast to the contribution of the interdecadal-trend component to the strength of strong El Niño events in which some enhance and some reduce the strength of El Niño events (Li et al., 2019). For the decay of the strong La Niña events in the boreal spring and early summer, the intraseasonal-interseasonal variations play a dominant role.

The La Niña event in 2020/2021 was successfully predicted by CFSv2 with a lead-time of half of a year. Nevertheless, the observed climate anomalies in the North American region are unexpected from the dynamic and statistic perspective, leading to unsuccessful predictions of climate anomalies in the region. That implies the important role of the internal dynamic or/and other processes in driving variability and low predictability in the North American region during winter 2020/2021.
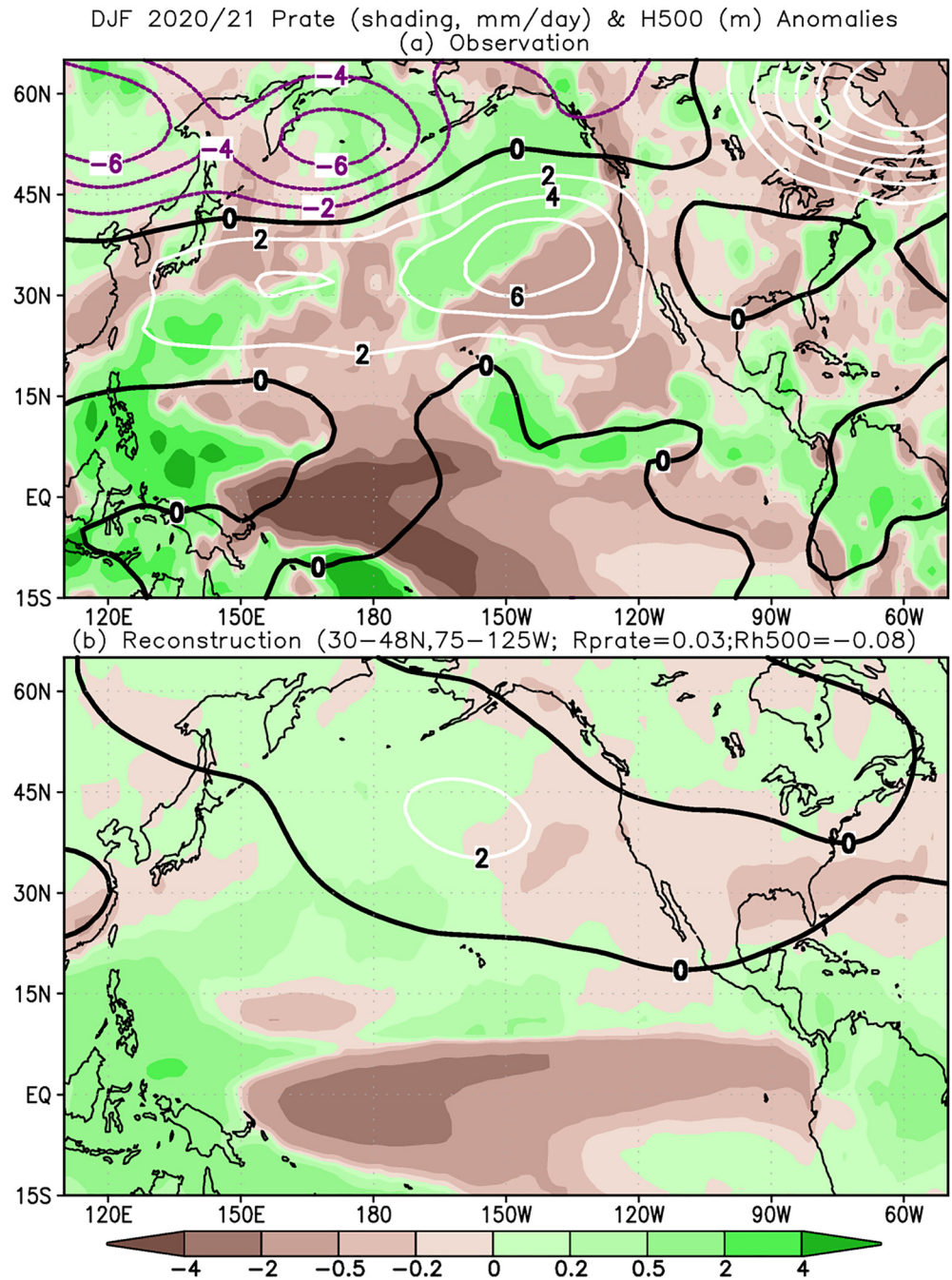
Figure 11. Observed (a) and reconstructed (b) geopotential height at 500 hPa (H500; contours; m) and precipitation (shading; mm/day) anomalies in December 2020–February 2021 (DJF 2020/21). The reconstructions are based on the regression onto the Niño3.4 index. The pattern correlations between the observations and the reconstruction are 0.03 for precipitation and −0.08 for H500 over the U. S (30°–48°N, 75°–125°W).

Data Availability Statement

Table 1

Heidke Skill Scores (HSS) of Three Categories of CPC Forecasts of Precipitation and Temperature in U. S. in DJF 2020/21: Non-Equal Chance Forecasts (Non-EC); All Forecasts; Percent Coverage of Not Equal Chance Forecasts (the Data From: https://www.cpc.ncep.noaa.gov/products/predictions/long_range/tools/briefing/seas_veri.grid.ph 639 p)

DJF 2020/21	Non-EC	All forecast	Percent coverage
Precipitation	−0.29	−0.22	74.14%
Temperature	−22.35	−17.24	77.16%

References

An, S.-I., Tziperman, E., Okumura, Y. M., & Li, T. (2020). ENSO Irregularity and asymmetry. In M. J. McPhaden, A. Santoso, & W. Cai (Eds.), *El Niño Southern Oscillation in a changing climate* (pp. 153–172). https://doi.org/10.1002/9781119548164.ch7

Behringer, D. W. (2007). The Global Ocean data assimilation system (GODAS) at NCEP. In *Preprints, 11th Symposium on Integrated Observing and similation systems for atmosphere, Oceans, and land surface*. American Meteorological Society. Retrieved from http://ams.confex.com/ams/87ANNUAL/techprogram/paper_119541.htm

Bjerknes, J. (1969). Atmospheric teleconnections from the equatorial Pacific. *Monthly Weather Review*, 97, 163–172. https://doi.org/10.1175/1520-0493(1969)097<0163:atftep>2.3.co;2

Chen, D., Lian, T., Fu, C., Cane, M. A., Tang, Y., Murtugudde, R., et al. (2015). Strong influence of westerly wind bursts on El Niño diversity. *Nature Geoscience*, 8, 339–345. https://doi.org/10.1038/ngeo2399

Chen, H.-C., Sui, C.-H., Tseng, Y.-H., & Huang, B. (2015). An analysis of the linkage of Pacific subtropical cells with the recharge–discharge processes in ENSO evolution. *Journal of Climate*, 28(9), 3786–3805. https://doi.org/10.1175/JCLI-D-14-00134.1

Chen, H.-C., Sui, C.-H., Tseng, Y.-H., & Huang, B. (2018). Combined role of high- and low-frequency processes of equatorial zonal transport in terminating an ENSO Event. *Journal of Climate*, 31(14), 5461–5483. https://doi.org/10.1175/jcli-d-17-0329.1

Chen, H.-C., Tseng, Y.-H., Hu, Z.-Z., & Ding, R. (2020). Enhancing the ENSO predictability beyond the spring barrier. *Scientific Reports*, 10(1), 1–12. https://doi.org/10.1038/s41598-020-57853-7

Clarke, A. J. (2010). Analytical theory for the quasi-steady and low-frequency equatorial ocean response to wind forcing: The 'tilt' and 'warm water volume' modes. *Journal of Physical Oceanography*, 40(1), 121–137. https://doi.org/10.1175/2009JPO4263.1

Clarke, A. J., & Gorder, S. V. (2001). ENSO prediction using an ENSO trigger and a proxy for Western equatorial Pacific warm pool movement. *Geophysical Research Letters*, 28(4), 579–582. https://doi.org/10.1029/2000gl012201

DiNezio, P. N., Deser, C., Okumura, Y., & Karspeck, A. (2017). Predictability of 2 year La Niña events in a coupled general circulation model. *Climate Dynamics*, 49(11), 4237–4261. https://doi.org/10.1007/s00382-017-3575-3

Harrison, D. E., & Vecchi, G. (1997). Surface westerly wind events in the tropical Pacific 1986-1995. *Journal of Climate*, 10, 3131–3156. https://doi.org/10.1175/1520-0442(1997)010<3131:wweitt>2.0.co;2

Hoerling, M., Kumar, A., & Zhong, M. (1997). El Niño, La Niña, and the nonlinearity of their teleconnections. *Journal of Climate*, 10(8), 1769–1786. https://doi.org/10.1175/1520-0442(1997)010<1769:enolna>2.0.co;2

Hu, S., & Fedorov, A. V. (2016). Exceptional strong easterly wind burst stalling El Niño of 2014. *Proceedings of the National Academy of Sciences of the United States of America*, 113(8), 2005–2010. https://doi.org/10.1073/pnas.1514182113

Hu, Z.-Z., Kumar, A., Huang, B., Zhu, J., L'Heureux, M., McPhaden, M. J., & Yu, J.-Y. (2020). The interdecadal shift of ENSO properties in 1999/2000: A review. *Journal of Climate*, 33(11), 4441–4462. https://doi.org/10.1175/JCLI-D-19-0316.1

Hu, Z.-Z., Kumar, A., Huang, B., Zhu, J., Zhang, R.-H., & Jin, F.-F. (2017). Asymmetric evolution of El Niño and La Niña: The recharge/discharge processes and role of the off-equatorial sea surface height anomaly. *Climate Dynamics*, 49(7–8), 2737–2748. https://doi.org/10.1007/s00382-016-3498-4

Hu, Z.-Z., Kumar, A., Jha, B., & Huang, B. (2020). How much of monthly mean precipitation variability over global land is associated with SST anomalies? *Climate Dynamics*, 54(1–2), 701–712. https://doi.org/10.1007/s00382-019-05023-5

Hu, Z.-Z., Kumar, A., Jha, B., Wang, W., Huang, B., & Huang, B. (2012). An analysis of warm pool and cold tongue El Niños: Air-sea coupling processes, global influences, and recent trends. *Climate Dynamics*, 38(9–10), 2017–2035. https://doi.org/10.1007/s00382-011-1224-9

Hu, Z.-Z., Kumar, A., Xue, Y., & Jha, B. (2014). Why were some La Niñas followed by another La Niña? *Climate Dynamics*, 42(3–4), 1029–1042. https://doi.org/10.1007/s00382-013-1917-3

Hu, Z.-Z., Kumar, A., Zhu, J., Huang, B., Tseng, Y.-h., & Wang, X. (2017). On the shortening of the lead time of ocean warm water volume to ENSO SST since 2000. *Scientific Reports*, 7(1), 1–7. https://doi.org/10.1038/s41598-017-04566-z

Hu, Z.-Z., Kumar, A., Zhu, J., Peng, P., & Huang, B. (2019). On the challenge for ENSO cycle prediction: An example from NCEP Climate Forecast System version 2. *Journal of Climate*, 32(1), 183–194. https://doi.org/10.1175/JCLI-D-18-0285.1

Huang, B., Hu, Z.-Z., Kennedy, J. J., & Zhang, H.-M. (2021). Sea Surface temperatures. [In "state of the climate in 2020"]. *Bulletin of the American Meteorological Society*, 102(8), S150–S153. https://doi.org/10.1175/2021BAMSStateoftheClimate.1

Huang, B., L'Heureux, M., Hu, Z.-Z., & Zhang, H.-M. (2016). Ranking the strongest ENSOs while incorporating SST uncertainty. *Geophysical Research Letters*, 43(17), 9165–9172. https://doi.org/10.1002/2016GL070888

Huang, B., L'Heureux, M., Lawrimore, J., Liu, C., Zhang, H.-M., Banzon, V., et al. (2013). Why did large differences arise in the sea surface temperature datasets across the tropical Pacific during 2012? *Journal of Atmospheric and Oceanic Technology*, 30(12), 2944–2953. https://doi.org/10.1175/JTECH-D-13-00034.1

Huang, B., Shin, C.-S., Shukla, J., Marx, L., Balmaseda, M., Halder, S., et al. (2017). Reforecasting the ENSO events in the past fifty-seven years (1958-2014). *Journal of Climate*, 30(19), 7669–7693. https://doi.org/10.1175/JCLI-D-16-0642.1

Huang, N. E., Shen, Z., Long, S. R., Wu, M. C., Shih, H. H., Zheng, Q., et al. (1998). The empirical mode decomposition and the Hilbert spectrum for nonlinear and non-stationary time series analysis. *Proceedings of the Royal Society of London. Series A: Mathematical, Physical and Engineering Sciences*, 454(1971), 903–993. https://doi.org/10.1098/rspa.1998.0193

Huang, N. E., & Wu, Z. (2008). A review on Hilbert-Huang transform: Method and its applications to geophysical studies. *Review of Geophysics*, 46(2), RG2006.

Iwakiri, T., & Watanabe, M. (2020). Multiyear La Niña impact on summer temperature over Japan. *Journal of the Meteorological Society of Japan*, 98, 1245–1260. https://doi.org/10.2151/jmsj.2020-064

Jin, F.-F. (1997a). An equatorial ocean recharge paradigm for ENSO. Part I: Conceptual model. *Journal of the Atmospheric Sciences*, 54(7), 811–829. https://doi.org/10.1175/1520-0469(1997)054<0811:aeorpf>2.0.co;2

Jin, F.-F. (1997b). An equatorial ocean recharge paradigm for ENSO. Part II: A stripped-down coupled model. *Journal of the Atmospheric Sciences*, 54(7), 830–847. https://doi.org/10.1175/1520-0469(1997)054<0830:aeorpf>2.0.co;2

Johnson, S. J., Stockdale, T. N., Ferranti, L., Balmaseda, M. A., Molteni, F., Magnusson, L., et al. (2019). SEAS5: The new ECMWF seasonal forecast system. *Geoscientific Model Development*, 12(3), 1087–1117. https://doi.org/10.5194/gmd-12-1087-2019

Kanamitsu, M., Ebisuzaki, W., Woollen, J., Yang, S. K., Hnilo, J. J., Fiorino, M., & Potter, G. L. (2002). NCEP-DOE AMIP-II reanalysis (r-2). *Bulletin of the American Meteorological Society*, 83(11), 1631–1643. https://doi.org/10.1175/BAMS-83-11-1631

Kessler, W. S. (2002). Is ENSO a cycle or a series of events? *Geophysical Research Letters*, *29*(23), 40. https://doi.org/10.1029/2002GL015924

Kumar, A., & Hu, Z.-Z. (2014). Interannual variability of ocean temperature along the equatorial Pacific in conjunction with ENSO. *Climate Dynamics*, *42*(5–6), 1243–1258. https://doi.org/10.1007/s00382-013-1721-0

Latif, M., Anderson, D., Barnett, T., Cane, M., Kleeman, R., Leetmaa, A., et al. (1998). A review of the predictability and prediction of ENSO. *Journal of Geophysical Research*, *103*(C7), 14375–14393. https://doi.org/10.1029/97JC03413

L'Heureux, M., Becker, E., Halpert, M. S., Hu, Z.-Z., MacRitchie, K., & Tippett, M. (2021). ENSO and the tropical Pacific. [In "state of the climate in 2020"]. *Bulletin of the American Meteorological Society*, *102*(8), S205–S210. https://doi.org/10.1175/2021BAMSStateoftheClimate.1

L'Heureux, M., Collins, D., & Hu, Z.-Z. (2013). Linear trends in sea surface temperature of the tropical Pacific Ocean and implications for the El Niño-Southern Oscillation. *Climate Dynamics*, *40*(5–6), 1223–1236. https://doi.org/10.1007/s00382-012-1331-2

Li, X., Hu, Z.-Z., & Huang, B. (2019). Contributions of atmosphere-ocean interaction and low-frequency variation to intensity of strong El Niño events since 1979. *Journal of Climate*, *32*(5), 1381–1394. https://doi.org/10.1175/JCLI-D-18-0209.1

Li, X., Hu, Z.-Z., Huang, B., & Jin, F.-F. (2020). On the interdecadal variation of the warm water volume in the tropical Pacific around 1999/2000. *Journal of Geophysical Research: Atmospheres*, *125*(18), e2020JD033306. https://doi.org/10.1029/2020JD033306

Liebmann, B., & Smith, C. A. (1996). Description of a complete (interpolated) outgoing long wave radiation dataset. *Bulletin of the American Meteorological Society*, *77*, 1275–1277. https://doi.org/10.1175/1520-0477-77.6.1274

MacLachlan, C., Arribas, A., Peterson, K. A., Maidens, A., Fereday, D., Scaife, A. A., et al. (2015). Global seasonal forecast System version 5 (GloSea5): A high-resolution seasonal forecast system. *Quarterly Journal of the Royal Meteorological Society*, *141*, 1072–1084. https://doi.org/10.1002/qj.2396

McPhaden, M. J. (2012). A 21st century shift in the relationship between ENSO SST and warm water volume anomalies. *Geophysical Research Letters*, *39*(9), L09706. https://doi.org/10.1029/2012GL051826

McPhaden, M. J., Santoso, A., & Cai, W. (2021). *El Niño southern oscillation in a changing climate. Geophysical monograph* (Vol. 253). American Geophysical Union, Wiley. https://doi.org/10.1002/9781119548164

McPhaden, M. J., & Zhang, X. (2009). Asymmetry in zonal phase propagation of ENSO sea surface temperature anomalies. *Geophysical Research Letters*, *36*, L13703. https://doi.org/10.1029/2009GL038774

Meinen, C. S., & McPhaden, M. J. (2000). Observations of warm water volume changes in the equatorial Pacific and their relationship to El Niño and La Niña. *Journal of Climate*, *13*(20), 3551–3559. https://doi.org/10.1175/1520-0442(2000)013<3551:oowwvc>2.0.co;2

National Research Council. (2010). *Assessment of intraseasonal to interannual climate prediction and predictability* (p. 192). The National Academies Press.

Okumura, Y. M., DiNezio, P., & Deser, C. (2017). Evolving impacts of multiyear La Niña events on atmospheric circulation and U.S. drought. *Geophysical Research Letters*, *44*. https://doi.org/10.1002/2017GL075034

Okumura, Y. M., Ohba, M., Deser, C., & Ueda, H. (2011). A proposed mechanism for the asymmetric duration of El Niño and La Niña. *Journal of Climate*, *24*(15), 3822–3829. https://doi.org/10.1175/2011JCLI3999.1

O'Lenic, E. A., Unger, D. A., Halpert, M. S., & Pelman, K. S. (2008). Developments in operational long-range climate prediction at CPC. *Weather and Forecasting*, *23*(3), 496–515. https://doi.org/10.1175/2007WAF2007042.1

Peng, P., Barnston, A. G., & Kumar, A. (2013). A comparison of skill between two versions of the NCEP Climate Forecast System (CFS) and CPC's operational short-Lead seasonal outlooks. *Weather and Forecasting*, *28*(2), 445–462. https://doi.org/10.1175/WAF-D-12-00057.1

Picaut, J., Ioualalen, M., Menkes, C., Delcroix, T., & McPhaden, M. J. (1996). Mechanism of the zonal displacements of the Pacific warm pool: Implications for ENSO. *Science*, *274*(5292), 1486–1489. https://doi.org/10.1126/science.274.5292.1486

Reynolds, R. W., Rayner, N. A., Smith, T. M., Stokes, D. C., & Wang, W. (2002). An improved in situ and satellite SST analysis for climate. *Journal of Climate*, *15*(13), 1609–1625. https://doi.org/10.1175/1520-0442(2002)015<1609:aiisas>2.0.co;2

Ropelewski, C., & Halpert, M. (1987). Global and regional scale precipitation patterns associated with the El Niño-Southern Oscillation. *Monthly Weather Review*, *115*(8), 1606–1626. https://doi.org/10.1175/1520-0493(1987)115<1606:garspp>2.0.co;2

Saha, S., Moorthi, S., Pan, H. L., Wu, X., Wang, J., Nadiga, S., et al. (2010). The NCEP climate forecast system reanalysis. *Bulletin of the American Meteorological Society*, *91*(8), 1015–1057. https://doi.org/10.1175/2010BAMS3001.1

Saha, S., Moorthi, S., Wu, X., Wang, J., Nadiga, S., Tripp, P., et al. (2014). The NCEP climate forecast system version 2. *Journal of Climate*, *27*, 2185–2208. https://doi.org/10.1175/JCLI-D-12-00823.1

Seo, K. H., & Xue, Y. (2005). MJO−related oceanic Kelvin waves and the ENSO cycle: A study with the NCEP Global Ocean data assimilation system. *Geophysical Research Letters*, *32*, L07712. https://doi.org/10.1029/2005GL022511

Timmermann, A., An, S. I., Kug, J. S., Jin, F. F., Cai, W., Capotondi, A., et al. (2018). El niño–southern oscillation complexity. *Nature*, *559*(7715), 535–545. https://doi.org/10.1038/s41586-018-0252-6

Tseng, Y.-H., Hu, Z.-Z., Ding, R.-Q., & Chen, H.-C. (2017). An ENSO prediction approach based on ocean conditions. *Climate Dynamics*, *48*(5–6), 2025–2044. https://doi.org/10.1007/s00382-016-3188-2

van Oldenborgh, G. J., Hendon, H., Stockdale, T., L'Heureux, M., de Perez, E. C., Singh, R., & van Aalst, M. (2021). Defining El Niño indices in a warming climate. *Environmental Research Letters*, *16*(4), 044003. https://doi.org/10.1088/1748-9326/abe9ed

Wu, X., Okumura, Y. M., Deser, C., & DiNezio, P. N. (2021). Two-year dynamical predictions of ENSO event duration during 1954–2015. *Journal of Climate*, *34*(10), 4069–4087. https://doi.org/10.1175/jcli-d-20-0619.1

Wu, X., Okumura, Y. M., & DiNezio, P. N. (2019). What controls the duration of El Niño and La Niña events? *Journal of Climate*, *32*, 5941–5965. https://doi.org/10.1175/jcli-d-18-0681.1

Wu, Z., & Huang, N. E. (2009). Ensemble empirical mode decomposition: A noise- assisted data analysis method. *Advances in Adaptive Data Analysis*, *1*, 1–41. https://doi.org/10.1142/S1793536909000047

Xie, P., & Arkin, P. A. (1997). Global precipitation: A 17-year monthly analysis based on gauge observations, satellite estimates, and numerical model outputs. *Bulletin of the American Meteorological Society*, *78*, 2539–2558. https://doi.org/10.1175/1520-0477(1997)078<2539:gpayma>2.0.co;2

Xue, Y., Chen, M., Kumar, A., Hu, Z.-Z., & Wang, W. (2013). Prediction skill and bias of tropical Pacific sea surface temperatures in the NCEP Climate Forecast System version 2. *Journal of Climate*, *26*(15), 5358–5378. https://doi.org/10.1175/JCLI-D-12-00600.1

Xue, Y., Huang, B., Hu, Z.-Z., Kumar, A., Wen, C., Behringer, D., & Nadiga, S. (2011). An assessment of oceanic variability in the NCEP climate forecast system reanalysis. *Climate Dynamics*, *37*(11–12), 2511–2539. https://doi.org/10.1007/s00382-010-0954-4

Yeo, S. R., Yeh, S. W., Kim, K. Y., & Kim, W. M. (2016). The role of low frequency variation in the manifestation of warming trend and ENSO amplitude. *Climate Dynamics*, *49*(4), 1197–1213. https://doi.org/10.1007/s00382-016-3376-0

Yu, J.-Y., & Fang, S.-W. (2018). The distinct contributions of the seasonal footprinting and charged-discharged mechanisms to ENSO complexity. *Geophysical Research Letters*, *45*, 6611–6618. https://doi.org/10.1029/2018gl077664

Zhang, R.-H., Zheng, F., Zhu, J., & Wang, Z. G. (2013). A successful real-time forecast of the 2010-11 La Niña event. *Scientific Reports*, *3*(1), 1–7. https://doi.org/10.1038/srep01108

Zhang, W.-J., Li, J.-P., & Jin, F.-F. (2009). Spatial and temporal features of ENSO meridional scales. *Geophysical Research Letters*, *36*, L15605. https://doi.org/10.1029/2009GL038672

Zhu, J., Kumar, A., Huang, B., Balmaseda, M. A., Hu, Z.-Z., Marx, L., & Kinter, J.-L. III. (2016). The role of off-equatorial surface temperature anomalies in the 2014 El Niño prediction. *Scientific Reports*, *6*(1), 1–8. https://doi.org/10.1038/srep19677